ADVANCED FUNCTIONAL MATERIALS
www.afm-journal.de

Vibration-Induced Deagglomeration and Shear-Induced Alignment of Carbon Nanotubes in Air

*Morteza Miansari, Aisha Qi, Leslie Y. Yeo, and James R. Friend**

Carbon nanotubes (CNTs) are widely known to agglomerate into difficult to separate, 10–100 μm bundles, even after suspension in solution. Here, a dry and rapid (≈10 s) method to deagglomerate bulk, unbound multi-walled CNT bundles due to surface acoustic waves (SAW) in a piezoelectric substrate is reported for the first time. The process first forms 1-μm CNT bundles from extremely large (≈10 Mm/s^2) mechanical accelerations due to the SAW; these bundles are consequently susceptible to SAW-induced evanescent, quasistatic electric fields that couple into the bundles and form a mat of long (1–10 μm) individual CNTs on the substrate surface. These CNTs may then be aligned along the direction of shear provided by sliding a glass cover slip 10 mm across the CNT mat. This alignment is notably independent of the SAW propagation direction. Further, the intrinsic structure of the nanotubes is unaffected as verified using Raman spectroscopy. Uniquely simple, the approach avoids the many shortcomings of other CNT deagglomeration techniques—particularly surface modification and suspension in solution—to rapidly separate and align large numbers of CNTs, thereby overcoming a key limitation in their use for a diverse range of applications.

1. Introduction

Multi-walled carbon nanotubes (MWNTs) are aggregated in their natural state after synthesis, and subsequent emulsification is a necessary step for their use in most industrial processes, not because of the specific application but because of their inevitable tendency to naturally agglomerate into ≈10 μm bundles due to the large inter-CNT van der Waals forces in addition to their extremely high aspect ratios and flexibility. Even in their dry state, these micro-scale bundle agglomerates nevertheless adversely affect the electronic structure of the individual MWNTs,[1] and, when used to fabricate composite materials, deliver only modest improvements in mechanical and electrical properties. As such, few, if any, of the advantages of individual isolated MWNTs potentially conferred to the material made from them can be achieved or exploited.[2–6] Consequently, direct use of nanotubes[7–10] in their intended application as deagglomerated MWNTs for mechanical stiffening and strengthening, conductivity control,[11] particularly in transparent media for the replacement of indium tin oxide as a nearly depleted resource,[12] and even respiratory studies[13,14] would streamline industrial processes and facilitate their broader use—without having to resort to fluid suspension, surfactants, and substantial processing as is generally required now.[15]

Many researchers have explored selective chemistries and mechanical techniques to obtain debundled CNTs to address the limitations associated with nanotube agglomeration. Selective chemical functionalization has commonly been used to improve the dispersion of the CNTs in different solvents and polymers. For instance, CNT solubility improves in organic solvents once they are covalently endowed with alkene functional groups[16–19] such as tetrahydrofuran, chloroform, dimethylformamide,[20] and methylene chloride.[21] Ultrasonication and ball milling, on the other hand, are straightforward approaches to break down CNT bundles, though at a cost: ultrasonication over long periods causes a significant increase in defects in the CNTs with an associated increase in the D band intensity (as measured by Raman spectroscopy) due to disordered sp^3 carbon.[22] In extreme cases, the graphene layers of the CNTs are completely destroyed and the nanotubes are converted into amorphous carbon nanofibers.[23] Furthermore, individual CNTs obtained by wet ultrasonication are usually very short,[24] only ≈10 to ≈100 nm in length. Ultrasonication also creates holes along the CNT side walls, resulting in "worm-eaten" damage.[25–27] Likewise, ball milling creates a large amount of amorphous carbon from CNT samples,[28,29] clearly indicating that the CNTs are damaged.

Once debundled, the orientation of the CNTs is important in most practical applications, and several methods have already been demonstrated to align the individually dispersed CNTs in a liquid medium. Some common methods include shear flows,[30,31] electric fields,[32–35] and magnetic fields,[36–39] all of which have limited alignment efficiency because of the rotation of CNTs due to fluid transport and Brownian motion of the CNTs in the fluid. Furthermore, chemical treatment of the CNTs are necessary to stabilize the dispersion, with surfactants

M. Miansari, A. Qi, L. Y. Yeo, J. R. Friend[+]
Micro/Nanophysics Research Laboratory
RMIT University
Melbourne, VIC 3000, Australia
E-mail: jfriend@eng.ucsd.edu
M. Miansari
Department of Mechanical and Aerospace Engineering
Monash University
Clayton, VIC 3800, Australia
[+]Present address: Department of Mechanical and Aerospace Engineering, University of California-San Diego, La Jolla, CA, 92122, USA

DOI: 10.1002/adfm.201402976

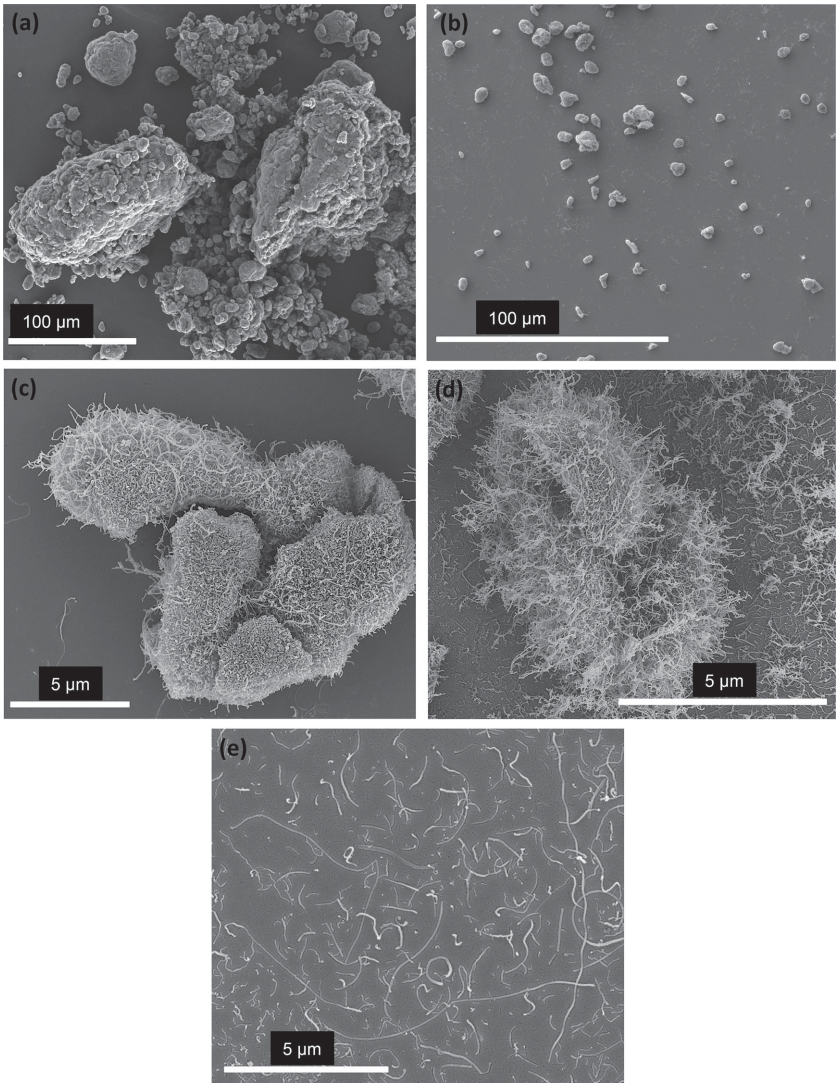

Figure 1. Deagglomeration of dry CNT bundles to form individual CNTs on a SAW device. Field-emission gun scanning electron microscopy (FEG-SEM) images of a) pristine CNTs including bundles of 100 μm and larger size. b) Small bundles (<10 μm) generated after 2 min of SAW exposure on a grounded 100 nm thick Au layer atop the lithium niobate substrate, preventing electric field interaction between the bundle and SAW. c) Large bundles ≈100 μm deagglomerate into smaller bundles via impact forces from mechanical vibration in the absence of electric field on the Au surface. d) Individual CNTs, appearing around the periphery are expelled from small 1–10 μm bundles like the one at the center due to Coulombic fission; and e) individual CNTs appear as a consequence on the lithium niobate surface after 10 s of SAW exposure.

or polymers required in typically complex, multistep chemical and physical processes.[16–21]

In this context, we report a simple, scalable, and rapid means to separate MWNTs from their bundles in their dry state. This is achieved without requiring suspension in solution nor the use of surfactants or any surface modification, instead only requiring surface acoustic wave (SAW) irradiation of the as-supplied dry bundled MWNTs, as illustrated in **Figure 1**, producing individual CNTs that are subsequently aligned using an applied shear force, thus overcoming the limitations of current approaches—even in comparison to other dry approaches that require substantial processing[40]—and presenting a direct method to produce oriented, individual CNTs. The method is explained in the following section, followed by experimental results that incorporate a simple analytical exploration of what mechanisms are responsible for their separation and alignment.

2. Materials and Methods

A SAW is a nanometer-order amplitude electromechanical wave that propagates along the surface of a single-crystal piezoelectric substrate.[41] The wave motion is trapped near the surface due to its relative slowness compared to the bulk wave speed, and is absent beyond about five wavelengths below the substrate surface, yet will propagate over thousands of wavelengths of distance—several centimeters—along the surface in a low-loss, single-crystal piezoelectric material such as lithium niobate ($LiNbO_3$ (LN), Roditi, London, UK). Patterned metal electrodes deposited directly onto the piezoelectric substrate—interdigital transducers(IDT), reported long ago by White and Voltmer[42] and depicted in **Figure 2**a, make the generation of SAW simple and straightforward. There are many kinds of SAWs, though by far the most commonly used for actuation is the Rayleigh wave,[43] a transverse-axial elliptical electroacoustic wave propagating at velocity $c_s = 3965$ m/s along the *x*-axis surface of an unloaded 127.68° *Y*-rotated cut, *X*-propagating LN substrate as shown in Figure 2a. The maximum particle velocity of the surface as the SAW passes is on the order of 1 m/s regardless of the excitation frequency, i.e., the SAW frequency. At 10-MHz order excitation frequencies, the wave amplitude is only of order 10 nm, but the acceleration of the surface is incredibly high, at around 10^8 m/s^2 or 10 million *g*'s. Such extreme surface accelerations are known to drive inertial behaviour in smoke nanoparticles in air that are bounced from the surface, forming patterns according to the SAW amplitude distribution.[44] SAW is furthermore known to align CNTs but only in suspension and with sufficient surfactant to prevent agglomeration.[45,46] We note the underlying mechanism for their alignment, arising from acoustic boundary layer streaming—the fluid flow in a thin submicron layer immediately adjacent to the substrate surface that is a consequence of its oscillation as the SAW traverses[47,48]—is entirely distinct from the dry-state deagglomeration mechanism due to mechanical impact and Coulombic fission. This mechanism and subsequent shear-driven alignment that we shall discuss below, is, to the best of our knowledge, the first time unbound CNT deagglomeration and alignment in the absence of solution has been reported.

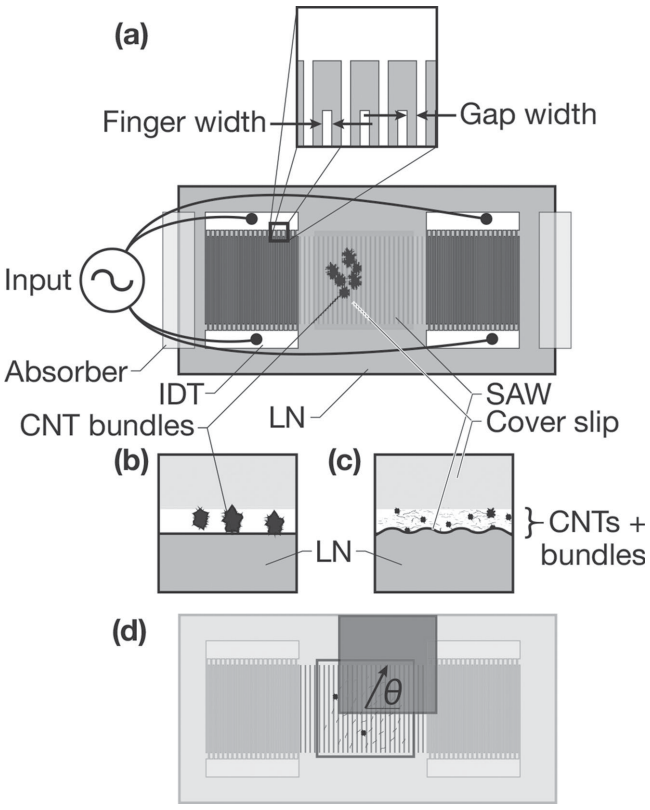

Figure 2. Schematic illustration of the deagglomeration of CNTs using the SAW. a) The SAW device, indicating the IDT electrode pair, the reflectors, and placement of the CNT bundles. b) From the side, but not to scale, the bundles are shown to be trapped by a glass cover slip as they are propelled and c) broken up into individual CNTs and smaller, broken bundles while remaining sandwiched in the gap between the glass cover slip and the substrate and exposed to the SAW. d) The alignment mechanism was determined by shearing the CNTs along an angle θ with respect to the SAW propagation direction by sliding the cover slip in this direction.

In the present work, a pair of simple Al–Cr IDTs were fabricated using sputter deposition (Hummer Sputter System, Anatech, Union City, CA) and standard UV photolithography with wet etching techniques onto 500 µm thick LN wafers; each IDT comprised 20 simple straight finger pairs with the gap and finger width each being a quarter of the SAW wavelength λ_{SAW} = 200 µm such that the fundamental Rayleigh wave mode's resonance frequency was f = 20 MHz given the value of c_s, as illustrated in Figure 2. Details of the fabrication procedure can be found elsewhere.[49,50] A radio frequency (RF) signal generator (N9310A, Agilent Technologies, Santa Clara, CA) and RF power amplifier (10W1000C, Amplifier Research, Bothell, WA) were used to drive both IDT electrodes at the resonance frequency, producing a standing Rayleigh SAW along the x-axis between the two IDTs. Outside these IDTs, a pair of α-gel (Oba Machinery, Shizuoka, Japan) absorbers were used to prevent edge reflections and the potential generation of spurious bulk waves.

In order to prevent loss of the MWNTs (www.cheaptubes.com) with average diameter and lengths below 50 nm and 10 µm, respectively, from the LN surface and to enhance deagglomeration and subsequent alignment, a glass cover slip (20 mm × 20 mm) (Figure 2b) was placed above the CNT bundles that were in turn deposited atop the LN substrate. A pressure of ≈10 kPa was applied to the top cover slip to compress the CNT bundles against the substrate. The motion of the CNT bundles was initially monitored using an optical microscope, revealing that the power required to drive debundling was at least 3 W; lower powers were found to produce no changes in the bundle shape or position. Increasing from 3 to 7 W, the CNT bundles were found to progressively deagglomerate faster and occur across a greater percentage of the bundles. Beyond 7 W, no improvement in the debundling was observed, and furthermore our devices tended to fail prematurely, making it often impossible to properly assess the deagglomeration results. The useful power for deagglomeration in our device was therefore estimated to be 3–7 W. While deagglomerating, a shear force parallel to the substrate surface was applied to the CNTs by sliding the cover slip over the LN and CNTs in a direction θ with respect to the SAW propagation over a distance of approximately 10 mm (Figure 2c), therefore leading to the alignment of individual CNTs; an XYZ translation stage with standard micrometers (Thorlabs, Newton, NJ) to which the cover slip was attached was used to provide all sliding motion. Scanning electron microscopy (Nova NanoSEM 450, FEI, Hillsboro, OR), image processing (MATLAB, Mathworks, Natick, MA), and micro-Raman spectroscopy (Confocal Micro-Raman Spectrometer (632.8 nm), Renishaw, Wotton-under-Edge, UK) were used to characterize the morphology and molecular structure of the results.

To determine the yield of the process in delivering individual CNTs from the bundles, image processing (**Figure 3**) was performed using custom MATLAB code with the regionprops function (Mathworks, Natick, MA),[51] incorporating statistical classification of the image components to separate out the bundles from individual CNTs. The area occupied by individual CNTs in each image is determined by thresholding the 255-greyscale SEM image (Figure 3a); "dark" pixels of greyscale value less than 127 were rendered white and the remainder black, thus inverting the consequent black and white image (Figure 3b). Pixels detected to be a part of a CNT bundle in white in Figure 3c were inverted to black in Figure 3d to remove them. At the magnification used here, the bundles were identified as objects possessing a contiguous area greater than 100 pixels (Figure 3c); if the magnification is altered, then obviously the threshold pixel count would need to be changed, though the difference between those pixels associated with an individual CNT and entire bundles is fairly obvious over a broad range of magnifications. By doing this, the projected area ratio of individual to bundled CNTs can be obtained, enumerating the CNTs in and out of the bundles if their respective densities are known.

3. Results and Discussion

3.1. SAW-Assisted CNT Deagglomeration

In pristine CNTs, bundles of different sizes are randomly formed due to the large van der Waals forces between the individual CNTs and also between the bundles themselves;

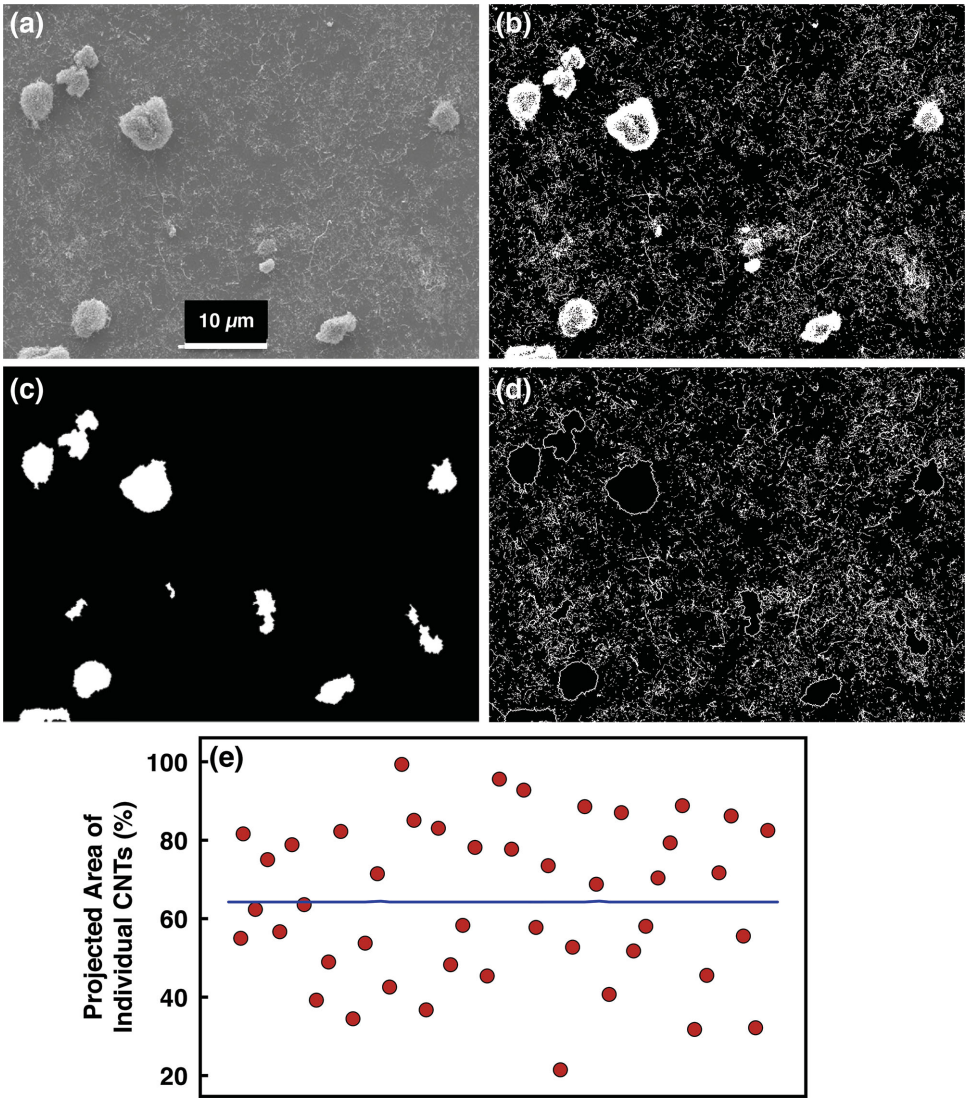

Figure 3. Detection of bundled and individual CNTs. a) Original, 256-grey SEM image, thresholded b) to a black and white image with 127 as the threshold; CNT bundles were identified as contiguous regions with more than 100 white pixels. d) Individual CNTs were identified through subtraction of these bundle regions from the image. e) The percentage of projected area by individual CNTs compared to the total projected area of CNTs, whether in a bundle or not, as calculated for 45 SEM images of the SAW deagglomeration results. On average (represented by the blue line), 64% of the CNT-filled area is occupied by free CNTs.

larger 100 μm bundles agglomerate from smaller bundles as depicted in Figure 1a: note how the large bundles in the image are actually composed of many, smaller (1–10 μm dimension) bundles. During SAW exposure, the large acceleration ($a_s \sim 10^8$ m/s^2) generated by the SAW perpendicular to the LN substrate causes a substantial impact force on the CNTs on every cycle of the SAW, equating to 20 million impacts per second. Such acceleration is known to cause inertial ejection of even nanoscale objects from the substrate surface, such as smoke particles.[44] The inertial forces responsible for the impact force may be estimated as $F_I \sim m_p a_s$, where m_p is the mass of the bundles. Thus, the larger the CNT bundle, the larger the impact force on that bundle; small bundles or individual CNTs may not be affected as strongly by impact due to their exceptionally low mass.

For the large bundles in Figure 1a, a simple experiment confirmed that mechanical impact was solely responsible for their breakup to smaller 1–10 μm bundles (Figure 1b). A grounded 100 nm Au layer was deposited on the LN device over several wavelengths and under the large CNT bundles to prevent exposure of the bundles to evanescent electric fields from the SAW such that the bundles were isolated from Coulombic forces and thus only subject to mechanical and intermolecular forces. We note that other forces arising due to the SAW may also be present on the CNT bundles, including acoustic radiation forces and acoustic streaming-driven drag forces, but it is evident from the comparison of force magnitudes in **Table 1** that for bundles ~10 μm and larger these are insignificant compared to the mechanical and intermolecular forces. The acoustic radiation force $F_R = -(\pi\, p_o^2 V_p \beta_m \varphi/2\lambda)\sin(4\pi x/\lambda$, in which ρ_m and β_m are the

Table 1. Forces acting on the bundles for four bundle sizes/diameters: 100 µm, 10 µm, 4 µm, and 1 µm. F_I, F_{vdW}, F_R, F_D, and F_E are the mechanical impact, van der Waals-mediated cohesive, acoustic radiation, acoustic streaming drag, and electric field forces acting on a bundle.

Bundle size (≈ diameter)	F_I	F_{vdW}	F_R	F_D	F_E
100 µm	10^{-2}	10^{-5}	10^{-16}	10^{-8}	10^{-8}
10 µm	10^{-5}	10^{-6}	10^{-19}	10^{-9}	10^{-10}
4 µm	10^{-6}	10^{-6}	10^{-20}	10^{-10}	10^{-11}
1 µm	10^{-8}	10^{-7}	10^{-22}	10^{-10}	10^{-12}

density and compressibility of the medium, that is, air, respectively, p_o the pressure amplitude, V_p the bundle volume, x the distance from a pressure node (e.g., $x = 100$ µm when located at a pressure antinode), ρ_p and β_p the density and compressibility of the bundle, respectively, and $\varphi = [(5\rho_p - 2\rho_m)/(2\rho_p + \rho_m)] - (\beta_p/\beta_m)$ the acoustic contrast factor,[52] is typically on the order of ~10^{-19} N for a 10 µm bundle. Likewise, the drag force on the CNT bundles due to acoustic streaming in air $F_D \sim \mu U R_o \sim 10^{-9}$ N,[44,53] where μ is the fluid viscosity and $U \sim 1$ m/s is the velocity of the surrounding fluid, is also insignificant.

After exposure to the SAW for about 2 minutes at ≈7 W power but with the 100 nm Au layer atop the device, all large bundles are observed to break up into much smaller 1–10 µm bundles as shown in **Figure 4**b, with the largest percentage of bundles having a radius of about 2–3 µm; this is also the size at which the impact forces on the bundle approach the magnitude of the adhesive van der Waals forces between the bundle and LN surface, where the bundles would be ejected from the surface during the vibration (see Figure 4c). To determine whether mechanical vibration is alone sufficient to break large bundles (≈100 µm), the energy density of mechanical impact forces during SAW irradiation, acting to break the bundles is compared with the cohesive van der Waals forces acting to retain the bundle size and CNTs within. For the impact forces, it is reasonable to assume the bundles possess spherical morphologies: while commercial CNT bundles are rarely spherical, possessing a rough surface morphology and being typically flattened into an oblong shape, a calculation of forces based on such irregular shaped particles is relatively complex and of questionable benefit given the statistical variation of size and characteristics from bundle to bundle. Presuming therefore that the large spherical CNT bundles are composed of CNTs of 20 nm mean diameter for simplicity, it is then possible to define and determine the impact energy density as the impact energy per unit volume of the bundle, $E_I = F_I d/V = \rho a_s d \sim 10^2 - 10^3$ Pa, where V is the bundle volume, ρ is the density of the CNTs, and $d \approx 10$ nm is an estimate of the displacement amplitude of the LN surface, based upon measurements from a Laser Doppler Vibrometer (LDV; MSA–400, Polytec, Waldbrunn, Germany). For van der Waals-mediated cohesion, we note that MWNTs usually form

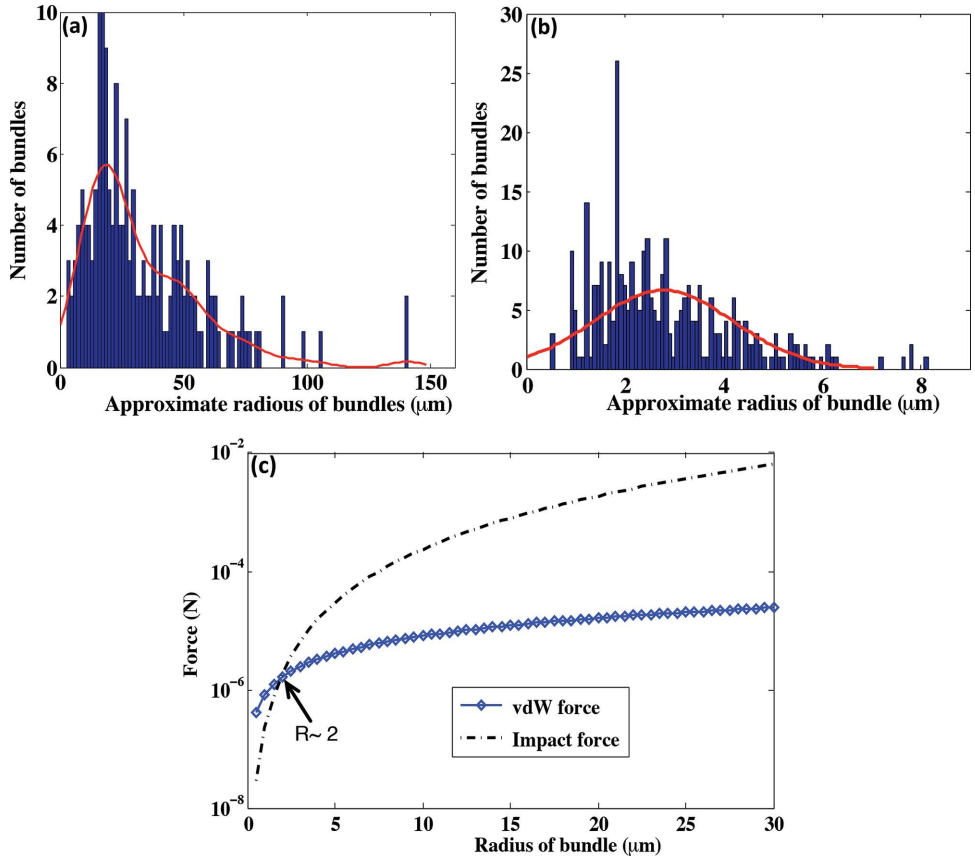

Figure 4. Histogram of the bundle size a) before and b) after 2 min exposure to SAW at 7 W power due to mechanical action alone. The electric field interaction was prevented using a grounded 100 nm thick Au layer atop the LN substrate. c) The impact and van der Waals forces[54] between the bundle and the surface of the LN substrate are similar when the radius of the bundle reaches ≈2 µm.

crossed mesh networks[53] with cohesive forces between them defined by the van der Waals binding energy at each contact junction between two CNTs of diameter D separated by a gap $H \approx 0.34$ nm that can be estimated as $E_{vdW} \sim -A_H D/12H$ for $H < D$,[53] where $A_H \approx 3.5$ eV is the Hamaker constant.[54] The cohesive energy density for the entire CNT network is then $E_C \sim c_t|E_{vdW}|$, where $c_t \sim 1/\xi^3$ is the number density of CNT contacts in the network with ξ being the spacing between the direct crossing junctions of the neighboring CNTs. Using SEM imagery, for example in Figure 1c, we estimate $\xi \sim 100$ nm,[53] thus giving $E_C \sim 10^3$ Pa, roughly the same order of magnitude as E_I, therefore suggesting that the impact alone is sufficient to deagglomerate the >10 µm large bundles into smaller 1–10 µm ones. The associated force values are provided in Table 1.

Nevertheless, without the Au layer, as in the case of all of the experiments reported with the sole exception described above to demonstrate the role of the mechanical force in breaking up the large 100 µm CNT bundles into smaller 1–10 µm bundles, a quasistatic[55] sinusoidal electric charge distribution is present on and evanescently above the bare LN substrate along which the SAW propagates, as illustrated in **Figure 5**. If the charging time is less than the time period associated with the SAW, $1/f$, local charge may then be injected into the conductive CNTs in contact with the substrate. Since a consequence of this quasistatic electric field means that the polarity of the induced charges on the CNTs depends on that of the substrate in direct contact with the CNTs in addition to the charging time, and since the latter at any given location along the SAW's propagation path reverses at a rate equivalent to the excitation frequency f,[56] electrostatic repulsion then arises due to matching charge polarity between the CNTs in a bundle. Here, we note that the time required to charge a single conductive CNT can be estimated as $\tau_c \sim \varepsilon_0\varepsilon_r/\sigma \sim 10^{-16}$ s, in which ε_r and σ are the relative permittivity and electrical conductivity of the CNT, respectively, and ε_0 is the permittivity of free space. Rather than attempt to guess the interconnectivity of the CNTs in the bundle, we take the worst-case scenario of a sufficient number of CNTs to form a bundle, but instead lined up end-to-end as one long line of CNTs, and examine the total time required to charge the CNT farthest from the charging source in the chain of CNTs: This amounts to approximately 10^{-12} s, five orders of magnitude smaller than the time period of the SAW, ~10^{-7} s, indicating that the charging is nearly instantaneous in comparison to the speed at which the charge reverses due to the SAW in the LN substrate, and thus suggesting that small CNT bundles <5 µm are completely charged in every half time period of the SAW, only to have that charge completely reversed in the next half time period.

In contrast to the large 100 µm bundles they originate from, the small 1–10 µm bundles that are broken from these large bundles due to the action of the mechanical impact arising from the SAW as described possess dimensions that are much smaller than the SAW wavelength, $\lambda/2 = 100$ µm, and therefore reside entirely in regions charged with the same polarity in every half time period of the SAW as it propagates along the piezoelectric substrate. The repulsive Coulombic force between the substrate and a CNT bundle of radius a_o is then $F_E \sim qE \sim 10^{-10}$ N, in which $q \approx 4\pi a_o^2 \varepsilon_0 E$ is the charge accumulated on the surface of the bundle and E is the electric field which can be estimated as the ratio of the voltage (≈20 V) applied to the IDTs to the finger width (50 µm) (Figure 2). We note that this repulsive electrostatic force, in contrast to the mechanical impact force, is insignificant compared to the cohesive van der Waals force[54] for the CNT network calculated above (Figure 4c) and therefore insufficient alone to break up large 100 µm bundles into smaller 1–10 µm bundles.

However, the internal electrostatic repulsion present between individual CNTs within the bundle due to their similar charges can nevertheless result in Coulombic fission of the smaller bundles, resulting in mass expulsion of CNTs from it, as shown in Figure 1d: a small 1–10 µm dimension CNT bundle in the center of the image appears to have lost large numbers of CNTs to the surrounding region with a characteristic gap between them, typical of bundles this size. Coulomb fission does not appear from large CNT bundles. Considering the Rayleigh instability limit at which the repulsive Coulomb energy is twice the cohesive binding energy, the potential required for Coulombic fission of two 3 µm long CNT strands with only one contact point is estimated to be ≈1 V.[57] The actual potential required for Coulombic fission in our experiments was however one magnitude greater, that is, ≈10 V, likely because the individual CNTs were entangled in a bundle with far more than one contact point. The rate of ejection of the CNTs via Coulombic fission is nevertheless directly dependent on the surface area to volume ratio, increasing linearly as the bundle size decreases. Fifty SEM images were analyzed to determine the typical size of bundles exhibiting Coulombic fission similar to that shown in Figure 1d; the majority of such bundles were between 1 and 4 µm in dimension suggesting therefore that Coulombic fission may be an effective means of completing the bundle breakup to form individual CNTs, because of both the continuous transmission of charge from the substrate into the bundle due to van der Waals-mediated adhesion (see Figure 4c), despite the presence and acceleration of the SAW, and the strength of the Coulombic fission at this

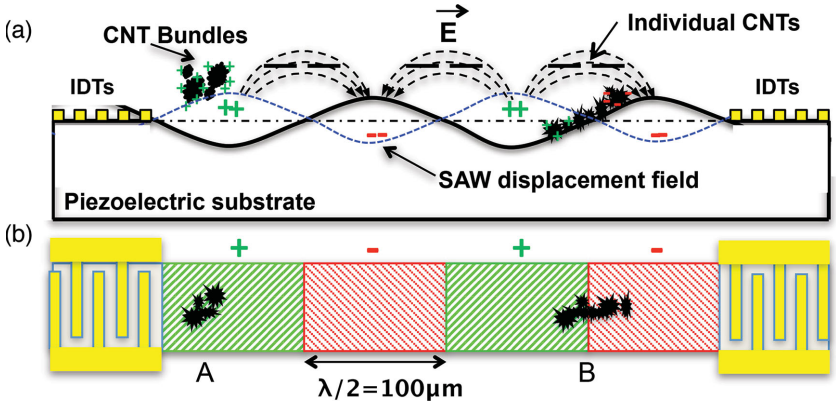

Figure 5. a) Side and b) top view illustrations of the instantaneous non-uniform charge distribution together with the mechanical displacement and electric field at a given time due to a standing wave SAW on the LN substrate.

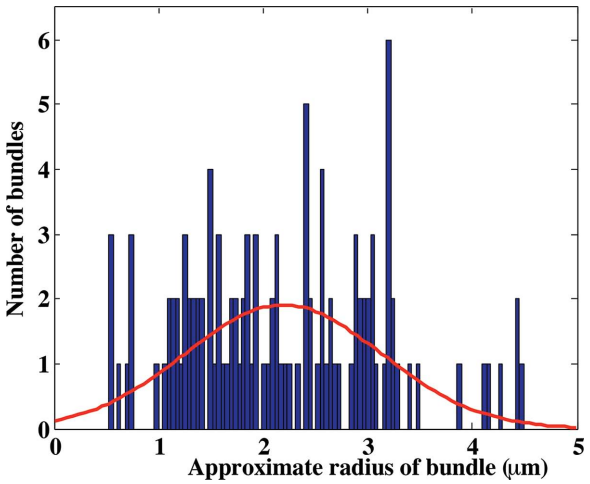

Figure 6. Size distribution of 50 different bundles that exhibited breakup to individual CNTs via Coulombic fission. Such events were narrowly limited to small bundles with dimensions of approximately 2 μm; no such events were seen for bundles larger than 4.5 μm.

length scale. In fact, **Figure 6** illustrates how CNT bundles of size greater than 4.5 μm do not exhibit Coulombic fission.

The reason this occurs is subtle: the charging of the bundles while in contact with the substrate. Regardless of bundle size, the mechanical impact force and the van der Waals-mediated cohesive force dominate all forces present on the bundle, as summarized in Table 1. As shown in Figure 4, 6, above the critical bundle size ≈4.5 μm the instantaneous impact force is dominant, ejecting the bundles from the substrate over each cycle of the SAW, permitting exceedingly brief electrical charging of the bundle per cycle. When the bundle is below this critical size the van der Waals force dominates, acting to keep these bundles onto the LN surface despite the extremely large surface acceleration. This allows the bundle to be continuously charged, driving Coulombic fission of CNTs from within the bundle and causing its eventual disintegration.

We also note from **Figure 7** that the standing wave nature of the SAW suggested in Figure 5 in this system is clearly evident

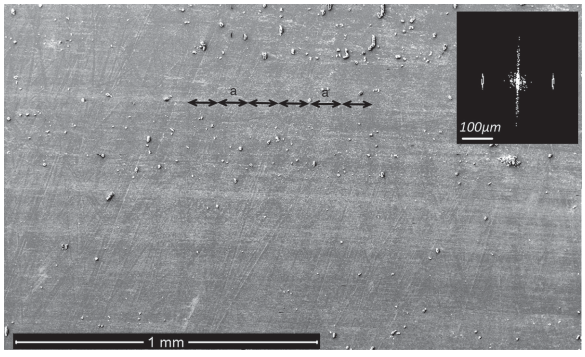

Figure 7. Individual CNTs are observed to form an uneven concentration pattern across the LN substrate after their expulsion due to Coulombic fission on a 20 MHz SAW device. The spacing between gaps in the CNT-rich regions $a = \lambda/2$—which appear lighter in grey in this image—was determined using direct measurement and fast Fourier transform (FFT; inset) of the SEM image.

through the periodicity of the CNTs after their expulsion. Individual CNTs are present in narrow regions separated by $a = \lambda/2$ along the propagation direction of the SAW and therefore due to the periodic electric field from the SAW, as determined by direct measurement and fast Fourier transform (FFT) of the image to expose the underlying order.

In summary, the SAW deagglomeration technique drives the formation of individual CNTs via impact breakup of the large 100 μm CNT bundles into smaller 1–10 μm bundles that subsequently eject individual CNTs as a consequence of Coulombic fission.

The efficiency of the process may be estimated by noting the density of free CNTs on the surface for a typical experiment, 1 CNT per 10 μm^2 (see Figure 1e for example), and the approximately 10 μm long CNTs remaining with a separation of $\xi \approx 100$ nm between them in the small, 10 μm sized bundles that we assume are nearly spherical (with therefore a volume of 10^{-18} m^3) and remain behind after SAW irradiation in some of our experiments. The CNTs within the bundle each occupy a volume of (10 μm) $\xi^2 \sim 10^{-20}$ m^3, and so each bundle has approximately 100 CNTs; given that each bundle occupies an area of (10~μm)^2, the areal density of CNTs in a bundle is 1 CNT/μm^2.

By determining the projected area of CNTs free on the surface versus those remaining in the CNT bundles, as provided in Figure 3e—an average of 64% over 45 SEM images across our experiments—roughly 10% of the CNTs are extracted from the bundles and left upon the surface. However, examining only our best five results from Figure 1e, where the conditions were especially favorable to freeing the individual CNTs from the bundles, fully 40% of the CNTs were freed from the bundles as indicated from 93% of the total CNT area on the substrate being occupied by individual CNTs. We have not attempted to separate the bundles from the individual CNTs, though this would be a feasible means to improve the final efficiency.

3.2. CNT Alignment

After the CNTs have been isolated on the substrate, an externally introduced shear force (Figure 2d) may be used to align them. While the alignment of nanowires has recently been studied[56] with alignment in a liquid medium along the SAW propagation direction, the CNTs in the present work can be aligned along any arbitrary direction while still in their dry state using only one pair of IDTs. After about 30 s of deagglomeration, the cover slip was brought down in contact with the substrate and clamped against the CNTs with an external pressure of approximately 10 kPa. Sliding the cover slip at an angle with respect to the SAW propagation over a distance of approximately 10 mm (see Figure 2) then produces a shear on the CNTs in the same direction.

To confirm the role of the shear in aligning the CNTs, we slid the cover slip at a specific angle θ with respect to the SAW propagation direction (Figure 2d) and examined the alignment of the CNTs from a series of SEM images collected during the process (see, for example, **Figure 8**), which were subsequently processed in a fashion similar to the method used to determine the deagglomeration mechanisms. Specifically, the white

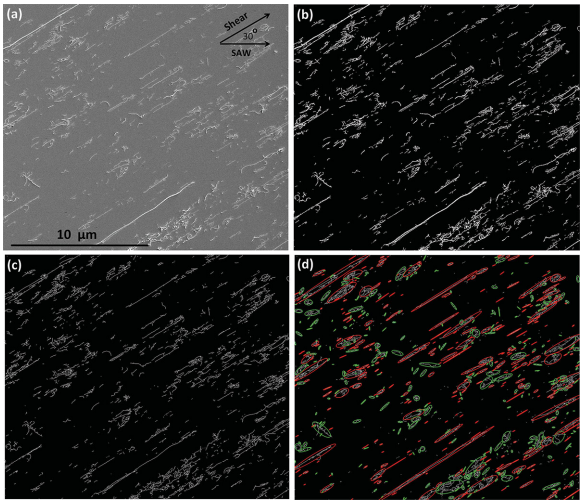

Figure 8. a) SEM image of the CNTs aligned under shear by sliding the cover slip atop the substrate and the CNTs along a direction at an angle ($\theta = 30°$) to the SAW propagation direction. b) Corresponding binary image and c) subsequent morphological thinning of the CNTs. d) SEM image of mainly randomly distributed CNTs: the red ellipses correspond to CNTs aligned along the shear direction whereas those in green correspond to unaligned CNTs.

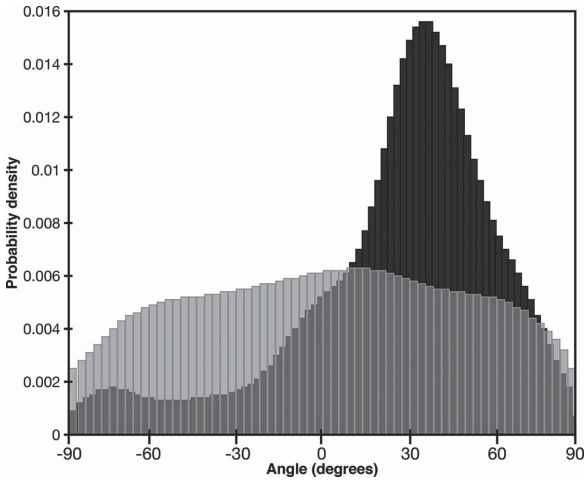

Figure 10. Probability density distribution of the angular deviation of the CNT orientation from the sliding direction. The grey distribution is due to deagglomeration and pressure without shear, while the black distribution represents cover-slip-driven shear at $\theta = 40°$.

traces that consequently represent the CNTs were converted into single-pixel wide lines in Figure 8c; this thinning provides a linear structure that indicates the direction along which the CNTs are oriented with the use of MATLAB and the regionprops function.[51] Figure 8d indicates the quality of the alignment: red ellipses define CNTs aligned, ±5°, along the shearing direction, corresponding to approximately 60% of the CNTs. The remaining 40% are not aligned and appear as green ellipses in the image.

Moreover, we also confirm from a probability density function of the angular deviation of the CNT orientation from the sliding direction in **Figure 9**, determined using a nonparametric kernel estimation function in MATLAB, detailed elsewhere,[58] that the CNT alignment is solely due to the sliding direction of the cover slip and hence the shear and not the SAW propagation: the angular deviation distribution is essentially identical regardless of the direction the shear is introduced—with respect to the SAW propagation direction—to align the CNTs. The correlation between the data can be quantified using Spearman's rank correlation coefficient[59] $R = 0.963$, very nearly one, therefore indicating that the sliding direction strongly defines the CNT alignment direction. This is further confirmed by the result shown in **Figure 10** in which the cover slip was held stationary: the unsheared CNTs exhibit a nearly uniform orientation—with perhaps a very weak alignment along the SAW wave propagation axis ($\theta = 0°$)—in comparison to the strong alignment exhibited by the CNTs under shear when the cover slip was moved.

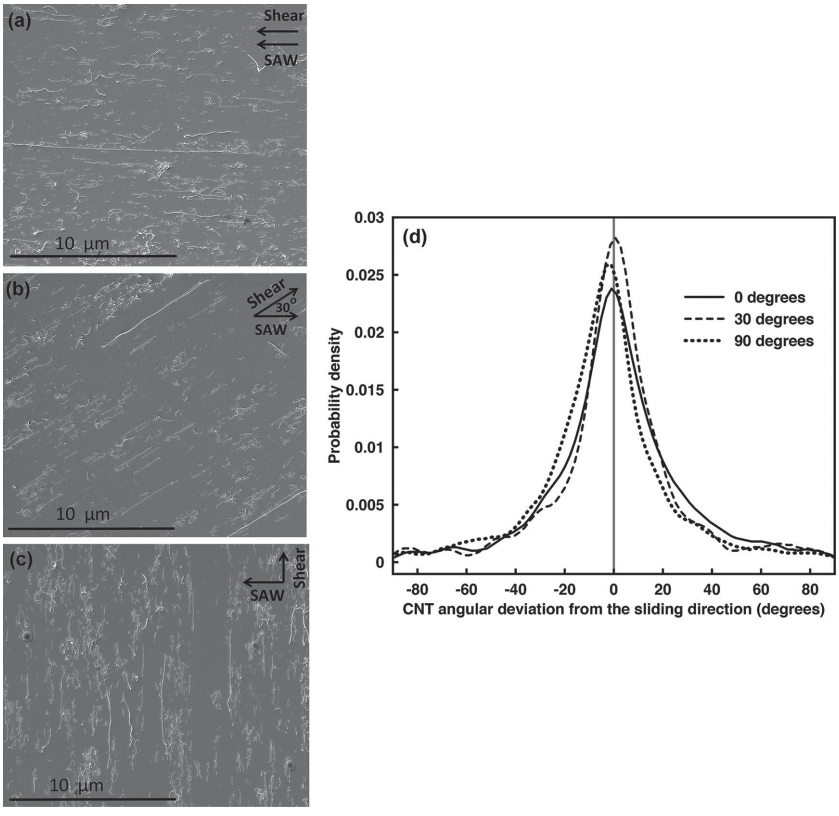

Figure 9. SEM images showing CNT alignment as a function of the shear axis with respect to the SAW propagation direction: a) $\theta = 0°$, b) $\theta = 30°$, and c) $\theta = 90°$. d) The probability density of a given CNT's angle with respect to the sliding direction is essentially invariant: the sole determinant of CNT alignment is the shear direction.

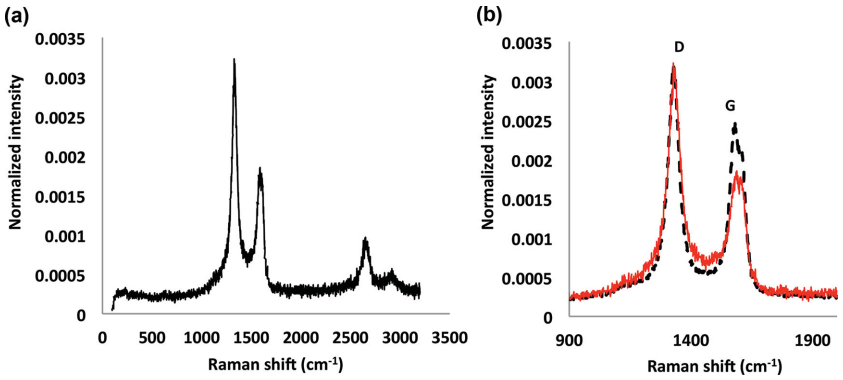

Figure 11. a) Raman spectra of pristine CNTs; b) a comparison of the normalized G and D bands for the CNTs before (red-solid line) and after (black-dash line) SAW exposure shows no apparent damage, but does indicate the increase in the number of individual CNTs.

3.3. Raman Spectra

The Raman spectra measured for as-provided CNTs and SAW-treated CNTs are presented in **Figure 11**. No increase in the intensity of the D band was observed, verifying that the deagglomeration of the CNT bundles produced by SAW has no influence on the chemical structure and does not damage the CNTs. On the other hand, the G band intensity increased by about 30 percent after SAW exposure, mainly because the bundled CNTs were deagglomerated and hence more individual CNTs contribute to the total G band intensity.

4. Conclusions

We demonstrate a method for rapid deagglomeration and alignment of aggregated MWNTs using surface vibrations on a piezoelectric substrate. Individual CNTs can be obtained through progressive bundle break-up of large 100 µm bundles into smaller 1–10 µm bundles from mechanical action via substrate ejection and impact due to the large surface accelerations associated with the SAW, and subsequently the ejection of individual CNTs from the smaller ≈1 µm-sized bundles due to Coulombic fission produced by the induced charging of the CNTs by the SAW-driven evanescent electric field of the substrate. Simultaneous alignment of the CNTs can be achieved through shear by sliding the cover slip atop the substrate, otherwise used to minimize loss of the CNTs to air, along a direction of the desired alignment. A convenient and useful forcing mechanism for rapid deagglomeration and alignment of CNTs, the whole process requires tens of seconds to complete, and the rate of production of the individual CNTs and small bundles for a single SAW device is ≈10 µg/min, which can be simply scaled up for high throughput processing by increasing the size of individual SAW devices and their number, the latter an elementary step as they are fabricated through standard mass microfabrication techniques. Currently 10% by number of CNTs are produced from the bundles across all our experiments, and our best results produce about 40% by number of CNTs free of the bundles. Regardless, the method breaks up all bundles to less than 10 µm in size. Scanning electron microscopy with associated image processing was used to characterize the SAW-assisted deagglomeration and alignment of the CNTs whereas Raman scattering spectroscopy indicated that the process did not damage the CNTs. The proposed SAW-assisted approach thus enables a broad swath of applications for deagglomeration of CNTs while avoiding drawbacks of other techniques. The simplicity of the technique further suggests that it may be scaled up to industrially relevant scales and likewise will be useful in the deagglomeration of other near-one-dimensional nanomaterials.

Acknowledgements

This work was performed in part at the Melbourne Centre for Nanofabrication (MCN), which is a node of the Australian National Fabrication Facility established under the National Collaborative Research Infrastructure Strategy to provide nano and micro-fabrication facilities for Australian researchers. L.Y.Y. acknowledges funding through an Australian Research Council Future Fellowship (FT130100672) whereas J.R.F. is grateful for Australian Research Council grants DP120100013 and DP120100835 in support of this work and RMIT University for a Vice-Chancellor's Senior Research Fellowship.

Received: August 28, 2014
Revised: November 2, 2014
Published online: December 15, 2014

[1] A. Rochefort, D. R. Salahub, P. Avouris, *Chem. Phys. Lett.* **1998**, *297*, 45–50.
[2] M. Noked, S. Okashy, T. Zimrin, D. Aurbach, *Angew. Chem.* **2012**, *124*, 1600–1603.
[3] Y. S. Song, J. R. Youn, *Carbon* **2005**, *43*, 1378–1385.
[4] J. Stein, B. Lenczowski, N. Fréty, E. Anglaret, *Carbon* **2012**, *50*, 2264–2272.
[5] G. L. Luque, N. F. Ferreyra, A. Granero, S. Bollo, G. A. Rivas, *Electrochim. Acta* **2011**, *56*, 9121–9126.
[6] P.-C. Ma, N. A. Siddiqui, G. Marom, J.-K. Kim, *Compos. Part A* **2010**, *41*, 1345–1367.
[7] A. Siria, P. Poncharal, A.-L. Biance, R. Fulcrand, X. Blase, S. T. Purcell, L. Bocquet, *Nature* **2013**, *494*, 455–458.
[8] R. Zhang, Y. Zhang, Q. Zhang, H. Xie, H. Wang, J. Nie, Q. Wen, F. Wei, *Nat. Commun.* **2013**, *4*, 1727.
[9] R. Singhal, Z. Orynbayeva, R. V. K. Sundaram, J. J. Niu, S. Bhattacharyya, E. A. Vitol, M. G. Schrlau, E. S. Papazoglou, G. Friedman, Y. Gogotsi, *Nat. Nanotechnol.* **2011**, *6*, 57–64.
[10] P. R. Smith, J. D. Carey, D. C. Cox, R. D. Forrest, S. R. P.Silva, *Nanotechnology* **2009**, *20*, 145202.
[11] J. Sung, J. Huh, J.-H. Choi, S. J. Kang, Y. S. Choi, G. T. Lee, J. Cho, J.-M. Myoung, C. Park, *Adv. Funct. Mater.* **2010**, *20*, 4305–4313.
[12] R. V. Salvatierra, C. E. Cava, L. S. Roman, A. J. G. Zarbin, *Adv. Funct. Mater.* **2013**, *23*, 1490–1499.
[13] Y. Fujitani, A. Furuyama, S. Hirano, *Aerosol Sci. Technol.* **2009**, *43*, 881–890.

[14] L. McJilton, C. Horton, C. Kittrell, D. Ogrin, H. Peng, F. Liang, W. E. Billups, H. K. Schmidt, R. H. Hauge, R. E. Smalley, *Carbon* **2009**, *47*, 2528–2530.
[15] S. H. Lee, D. H. Lee, W. J. Lee, S. O. Kim, *Adv. Funct. Mater.* **2011**, *21*, 1338–1354.
[16] J. Chen, M. A. Hamon, H. Hu, Y. Chen, A. M. Rao, P. C. Eklund, R. C. Haddon, *Science* **1998**, *282*, 95–98.
[17] J. Chen, H. Liu, W. A. Weimer, M. D. Halls, D. H. Waldeck, G. C. Walker, *J. Am. Chem. Soc.* **2002**, *124*, 9034–9035.
[18] M. Holzinger, O. Vostrowsky, A. Hirsch, F. Hennrich, M. Kappes, R. Weiss, F. Jellen, *Angew. Chem., Int. Ed.* **2001**, *40*, 4002–4005.
[19] V. Georgakilas, K. Kordatos, M. Prato, D. M. Guldi, M. Holzinger, A. Hirsch, *J. Am. Chem. Soc.* **2002**, *124*, 760–761.
[20] S. Banerjee, S. S. Wong, *Nano Lett.* **2002**, *2*, 49–53.
[21] P. Boul, J. Liu, E. Mickelson, C. Huffman, L. Ericson, I. Chiang, K. Smith, D. Colbert, R. Hauge, J. Margrave, *Chem. Phys. Lett.* **1999**, *310*, 367–372.
[22] K. Lu, R. Lago, Y. Chen, M. Green, P. Harris, S. Tsang, *Carbon* **1996**, *34*, 814–816.
[23] K. Mukhopadhyay, C. D. Dwivedi, G. N. Mathur, *Carbon* **2002**, *40*, 1373–1376.
[24] K. J. Ziegler, Z. Gu, J. Shaver, Z. Chen, E. L. Flor, D. J. Schmidt, C. Chan, R. H. Hauge, R. E. Smalley, *Nanotechnology* **2005**, *16*, S539–S544.
[25] H. Yanagi, E. Sawada, A. Manivannan, L. A. Nagahara, *Appl. Phys. Lett.* **2001**, *78*, 1355–1357.
[26] M. Yudasaka, M. Zhang, C. Jabs, S. Iijima, *Appl. Phys. A* **2000**, *71*, 449–451.
[27] M. Zhang, M. Yudasaka, A. Koshio, C. Jabs, T. Ichihashi, S. Iijima, *Appl. Phys. A: Mater. Sci. Proc.* **2002**, *74*, 7–10.
[28] Y. Li, B. Wei, J. Liang, Q. Yu, D. Wu, *Carbon* **1999**, *37*, 493–497.
[29] M. Haluska, M. Hulman, M. Hirscher, M. Becher, S. Roth, I. Stepanek, P. Bernier, Hydrogen storage in mechanically treated single wall carbon nanotubes. Electronic Properties of Nanostructures: XV International Winterschool/Euroconference, Kirchberg, Austria **2001**, pp 603–608.
[30] Z. Fan, S. G. Advani, *Polymer* **2005**, *46*, 5232–5240.
[31] S. Pujari, S. S. Rahatekar, J. W. Gilman, K. K. Koziol, A. H. Windle, W. R. Burghardt, *J. Chem. Phys.* **2009**, *130*, 214903–9.
[32] X. Chen, T. Saito, H. Yamada, K. Matsushige, *Appl. Phys. Lett.* **2001**, *78*, 3714–3716.
[33] K. Yamamoto, S. Akita, Y. Nakayama, *Jpn. J. Appl. Phys.* **1996**, *35*, L917–L918.
[34] K. Bubke, H. Gnewuch, M. Hempstead, J. Hammer, M. L. Green, *Appl. Phys. Lett.* **1997**, *71*, 1906–1908.
[35] J. Chung, K.-H. Lee, J. Lee, R. S. Ruoff, *Langmuir* **2004**, *20*, 3011–3017.
[36] K. Kordás, T. Mustonen, G. Tóth, J. Vähäkangas, A. Uusimäki, H. Jantunen, A. Gupta, K. Rao, R. Vajtai, P. M. Ajayan, *Chem. Mater.* **2007**, *19*, 787–791.
[37] G. Korneva, H. Ye, Y. Gogotsi, D. Halverson, G. Friedman, J.-C. Bradley, K. G. Kornev, *Nano Lett.* **2005**, *5*, 879–884.
[38] S. C. Youn, D.-H. Jung, Y. K. Ko, Y. W. Jin, J. M. Kim, H.-T. Jung, *J. Am. Chem. Soc.* **2008**, *131*, 742–748.
[39] M. A. Correa-Duarte, M. Grzelczak, V. Salgueiriño-Maceira, M. Giersig, L. M. Liz-Marzan, M. Farle, K. Sierazdki, R. Diaz, *J. Phys. Chem. B* **2005**, *109*, 19060–19063.
[40] C. Feng, K. Liu, J.-S. Wu, L. Liu, J.-S. Cheng, Y. Zhang, Y. Sun, Q. Li, S. Fan, K. Jiang, *Adv. Funct. Mater.* **2010**, *20*, 885–891.
[41] J. Friend, L. Y. Yeo, *Rev. Mod. Phys.* **2011**, *83*, 647–704.
[42] R. White, F. Voltmer, *Appl. Phys. Lett.* **1965**, *7*, 314–316.
[43] J. W. Strutt, *Proc. London Math. Soc.* **1885**, *4*, S1–S17.
[44] M. K. Tan, J. R. Friend, L. Y. Yeo, *Appl. Phys. Lett.* **2007**, *91*, 224101–3.
[45] T. Smorodin, U. Beierlein, J. Ebbecke, A. Wixforth, *Small* **2005**, *1*, 1188–1190.
[46] K. M. Seemann, J. Ebbecke, A. Wixforth, *Nanotechnology* **2006**, *17*, 4529–4532.
[47] A. R. Rezk, O. Manor, J. R. Friend, L. Y. Yeo, *Nat. Commun.* **2012**, *3*, 1167.
[48] O. Manor, L. Y. Yeo, J. R. Friend, *J. Fluid Mech.* **2012**, *707*, 482–495.
[49] H. Li, J. R. Friend, L. Y. Yeo, *Biomed. Microdevices* **2007**, *9*, 647–656.
[50] M. K. Tan, J. R. Friend, L. Y. Yeo, *Lab Chip* **2007**, *7*, 618–625.
[51] S. Eddins, Visualizing regionprops ellipse measurements, 2010; http://blogs.mathworks.com/steve/2010/07/30/visualizing-region-props-ellipse-measurements/ (accessed: March, 2014).
[52] J. Nam, Y. Lee, S. Shin, *Microfluid. Nanofluid.* **2011**, *11*, 317–326.
[53] Y. Y. Huang, E. M. Terentjev, *Polymers* **2012**, *4*, 275–295.
[54] R. Lee-Desautels, *Educ. Reso. for Part. Techn.* **2005**, 1–8.
[55] B. Auld, *Acoustic Fields and Waves in Solids*, Vol. 1 and 2, Wiley, Somerset, NJ, USA **1973.**
[56] Y. Chen, X. Ding, S.-C. Steven Lin, S. Yang, P.-H. Huang, N. Nama, Y. Zhao, A. A. Nawaz, F. Guo, W. Wang, *ACS Nano* **2013**, *7*, 3306–3314.
[57] G. Liu, Y. Zhao, K. Zheng, Z. Liu, W. Ma, Y. Ren, S. Xie, L. Sun, *Nano Lett.* **2008**, *9*, 239–244.
[58] V. A. Epanechnikov, *Theory Probab. Its Appl.* **1969**, *14*, 153–158.
[59] C. Spearman, *Am. J. Psychol.* **1904**, *15*, 72–101.